JOURNAL OF MATERIALS SCIENCE, 30 (1995) 3291–3299

Grain size effects on cyclic fatigue and crack-growth resistance behaviour of partially stabilized zirconia

M. J. HOFFMAN*, YIU-WING MAI
Centre for Advanced Materials Technology, Department of Mechanical Engineering, University of Sydney, Sydney, NSW 2006, AUSTRALIA

R.H. DAUSKARDT
Department of Materials Science and Engineering, Stanford University, Stanford, CA 94305-2205, USA

J. AGER, R.O. RITCHIE
Center for Advanced Materials, Materials Sciences Division, Lawrence Berkeley Laboratory and Department of Materials Science and Mineral Engineering, University of California, Berkeley, CA 94720, USA

Cyclic fatigue crack growth and crack-resistance behaviour was studied in partially stabilized zirconia (PSZ) with three different cubic-phase grain sizes following sub-eutectoid heat treatments. Raman spectroscopy was used to determine the extent of phase transformation around the cracks for both cyclic and monotonic loading conditions. All tests were on "long", through thickness cracks using compact-tension specimens. Predictions of crack-tip shielding were made following determination of toughening parameters using crack-resistance data. It was found that the dominant factors affecting cyclic fatigue-crack growth were the level of crack-tip shielding, as a result of phase transformation, and the intrinsic toughness of the material. Grain size did not appear to significantly affect fatigue crack-growth behaviour.

1. Introduction

Despite initial observations to the contrary [1, 2], the phenomenon that ceramic materials are susceptible to strength degradation under cyclic loading is now well documented. Such degradation has been assumed to occur due to hysteretic processes occurring at the crack tip. In fact, extensive studies, undertaken on a wide range of these materials including aluminas [3–5], silicon nitrides [6] and zirconia ceramics [7–9], clearly show reduced lifetimes under cyclic, compared to quasi-static, loading. While initial evidence for cyclic fatigue degradation was based solely upon strength data, more recent studies have shown significantly enhanced crack-growth rates under cyclic loading, combined with much lower fatigue thresholds, than measured under sustained loads [9, 10].

The purpose of this paper is to study the effect of different grain sizes on cyclic fatigue crack growth and crack-resistance (R-curve) behaviour in magnesia-containing partially stabilized zirconia (Mg–PSZ). The cyclic fatigue and crack-resistance behaviour of three different grain sizes of PSZ following two different sub-eutectoid ageing cycles are investigated. The extent of crack-tip shielding as a result of transformation toughening is estimated from the R-curve data; transformation-zone sizes were determined using Raman spectroscopy. Crack-growth rates as a function of the stress intensity at the crack tip are deduced to clarify further the role of the grain size on fatigue behaviour.

2. Micromechanisms for cyclic fatigue

While the occurrence of cyclic fatigue damage has frequently been reported, the microstructural damage and crack-advance mechanisms involved are not as yet fully documented. In alumina and silicon nitride ceramics, for example, *in situ* observations [5], coupled with extensive theoretical modelling [11–14], have led to the identification of a mechanical fatigue mechanism. Toughening in these materials occurs by grain bridging; repetitive sliding of the grain interfaces under cyclic loading, however, leads to frictional degradation and a reduced shielding capacity of the grain bridging zone. Such extrinsic mechanisms for fatigue-crack growth, involving the cyclically-induced

* *Present address*: FG Nichtmetallisch-Anorganische Werkstoffe, TH Darmstadt, Hilpertsr. 31; Darmstadt 64295, Germany.

0022–2461

degradation of crack-tip shielding mechanisms, may be expected in other materials such as fibre-reinforced composites.

In contrast, the micromechanisms responsible for cyclic fatigue damage in phase-transforming ceramics are not clearly understood. *In situ* studies on Mg–PSZ in a scanning electron microscope (SEM) [15] have shown the formation of "slip lines" at the crack-tip during cyclic loading; crack propagation was proposed to occur along these slip bands in a process similar to that occurring in metals. This process involves the concept of crack extension by alternating crack-tip blunting and resharpening which, although conceivable, has not been confirmed in ceramic materials. A number of authors have observed the formation of fatigue striations or crack arrest markings on fracture surfaces in Mg–PSZ [15] and tetragonal zirconia phase (TZP) [16] ceramics, which would be consistent with the notion that crack advance occurs via a mechanism similar to that in metals.

The presence of uncracked ligament bridging has also been shown to occur during crack growth in Mg–PSZ [17] (Fig. 1). Under cyclic loading, these bridges may suffer progressive wear degradation reducing their capacity to shield the crack tip. Such ligaments appear to form as a result of microcracks developing ahead of the crack tip which fail to link with the main crack (Fig. 2). The presence of such microcracks can be enhanced if blunting of the crack tip (e.g. by slip-band formation) occurs, as the location of the maximum principal stress is at roughly two crack-opening displacements ahead of the tip [18]. Such behaviour is well documented for metal–matrix composites [19].

Compliance changes in uniaxially cyclically loaded samples have been suggested as evidence for the formation of microcracks in Y–TZP under cyclic loading [16, 20]. Specifically, crack initiation occurs at pre-existing flaws, either in the bulk or surface of the material; localized stresses around these flaws then promote microcrack nucleation and coalescence causing lower failure strengths under cyclic load. Microcracks in zirconia toughened alumina (ZTA), Mg–PSZ and Y–TZP have also been observed using transmission electron microscopy [21]; their formation has been attributed to either large residual stresses as a result of martensitic transformation or elastic anisotropy [22].

However, if phase-transformation toughening is the sole shielding (toughening) mechanism in zirconia ceramics, the primary mechanism of cyclic fatigue is likely to be *intrinsic*, i.e. propagation along transformation bands or accumulation of microcracks. Initial observations using Raman spectroscopy [10, 23] have shown that the size of transformed zones around cracks, and hence the extent of transformation toughening, is solely a function of the maximum applied load at the crack tip and is unaffected by cyclic loading; reorientation of transformation strains under cyclic loads has not been observed [10]. Conversely, if other toughening mechanisms are present, such as crack bridging, it is possible that cyclic fatigue may involve an *extrinsic* component such as accelerated bridge degradation under alternating loads.

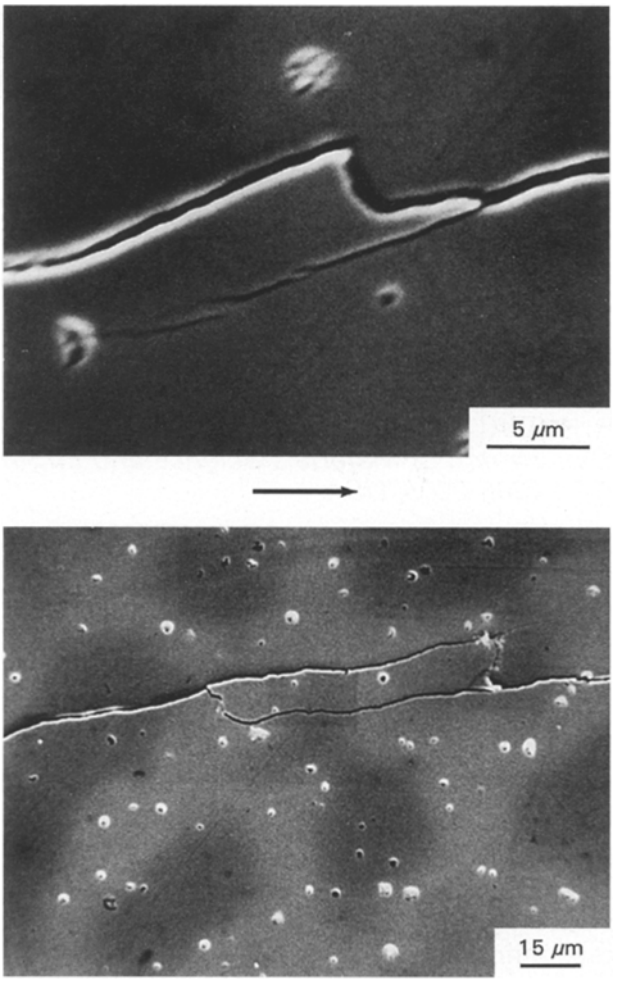

Figure 1 Examples of uncracked ligament bridges just behind the tip of fatigue cracks in TS grade Mg–PSZ during cyclic loading. Arrow indicates direction of crack growth.

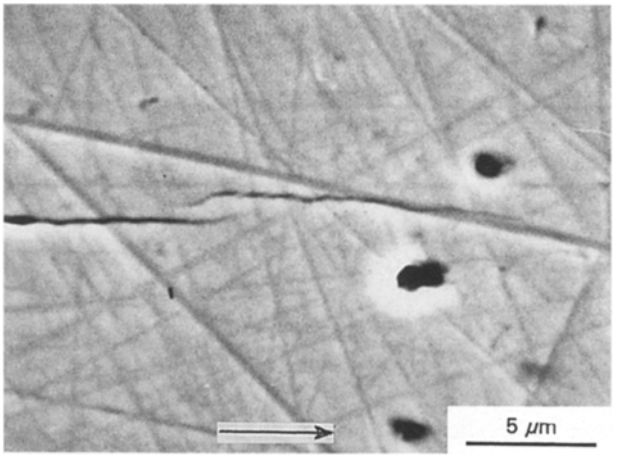

Figure 2 Uncracked bridging ligament formed by microcracking ahead of the crack tip in TS grade Mg–PSZ.

Only limited work has been performed on the effects of grain size on cyclic fatigue–crack growth in ceramic materials. In alumina, studies [24, 25] have shown that lifetimes under cyclic loads are reduced as grain size is increased, although the larger grain size might be expected to induce more grain bridging. The effect of changing grain size on cyclic fatigue has been studied in TZP. In Y–TZP [26], it has been shown that under both cyclic and static loading, strength

decreases with increasing grain size; however, as grain size increased, so did porosity with a subsequent decrease in the inert strength. When fatigue strength was normalized with inert strength, lifetimes under cyclic load were found to increase with grain size. Crack-growth data under cyclic fatigue have been obtained for four different grain sizes in Ce–TZP [27] where it was found that crack-growth rates decreased with increasing grain size. Here the level of crack-tip shielding, as evidenced by the size of the transformed zone around the crack, increased with increasing grain size, thereby providing an explanation for the observed grain-size effects under cyclic loading.

3. Experimental procedures

3.1. Materials

Mg–PSZ materials of 32, 50 and 100 μm grain size (cubic phase) were used in this study. These had been aged initially to a peak strength (MS grade) condition. A subsequent heat treatment by sub-eutectoid ageing was then performed on half of the samples to the peak toughness (TS grade) condition, which induced greater transformation toughening. All the samples had a Young's modulus of $E = 207$ GPa and a Poisson's ratio of $\nu = 0.31$. In this paper, the nomenclature used will consist of the grain size of the material followed by the heat treatment condition, e.g. 100 TS for the 100 μm grain size material with TS grade heat treatment. For both the cyclic fatigue and crack-resistance curve tests, crack-growth data were obtained with "long" cracks (of length in excess of ~2 mm) using compact-tension C(T) samples with a thickness of 3 mm and a cross section of 50×50 mm^2.

3.2. Mechanical testing

Applied stress intensities, K, were obtained for the C(T) geometry from handbook solutions [28], namely

$$K = \frac{P(2W + a)}{B(W - a)^{3/2}} F\left(\frac{a}{W}, \frac{b}{W}, \frac{c}{W}\right) \quad (1)$$

where P is the applied load, a the crack length, W the specimen width, B the specimen thickness and b and c the loading-pin hole diameter and location. Specimens were not of a standard size with $b/W = 0.625$ and $c/W = 0.345$; F was therefore obtained by interpolating between known values of standard specimens as

$$F = 8.875\left(\frac{a}{W}\right)^5 - 31.008\left(\frac{a}{W}\right)^4 + 41.603\left(\frac{a}{W}\right)^3 - 26.068\left(\frac{a}{W}\right)^2 + 7.189\left(\frac{a}{W}\right) + 0.736 \quad (2)$$

Equation 2 is accurate to within 0.3% for $0.2 \leq a/W \leq 1.0$. Both sides of the sample were polished to ~1 μm finish and a NiCr film of ~0.2 μm thickness evaporated onto one side to measure crack lengths. By monitoring the electrical-potential change across this crack-length gauge with crack extension, it was possible to determine crack lengths with a resolution of ± 2 μm.

Tests were performed on an MTS servohydraulic load frame and controller at a cyclic frequency of 25 Hz (sine wave) and load ratio R ($= K_{min}/K_{max}$) of 0.1 in ambient temperature air. Crack growth was initiated from the half chevron notch and grown for ~2–3 mm under cyclic load from the notch region. Tests were subsequently run under computer control to enable the applied stress intensities to be decreased at a controlled rate as a function of crack length, thus eliminating the effects of loading history on crack-growth rates. Consistency of the data was checked in two specimens by repeating the decreasing portion of the test three times; in all cases, results were reproducible.

Following the cyclic fatigue tests, the size of the transformed zone around the crack was determined using spatially resolved Raman spectroscopy, which allowed determination of the extent of transformation of the tetragonal to monoclinic phase. Details of the procedures are described below. Test samples were then heat treated at 800 °C for approximately 10 min to retransform the monoclinic phase near the crack back to its original tetragonal phase. This was undertaken in an inert helium environment to ensure that the NiCr crack-length gauge did not deteriorate. Subsequently, crack-resistance curve tests were performed by loading the samples under displacement control and crack length versus applied load was recorded; in this manner, crack extension, Δa, versus K_R plots were obtained (using Equation 1) for cracks grown from a pre-crack in nominally *untransformed* material. The size of the transformed zone due to monotonic loading was then determined by Raman spectroscopy.

3.3. Transformation Zone Measurements

The method used to perform spatially resolved Raman spectroscopy has been described in detail previously [29–31]; only a brief description will be given here. The expanded beam of an Ar-ion laser (488 nm), incident 65° from the surface normal, was focused onto the sample using a cylindrical lens, forming a slit-like illuminated area, 9 mm high and 25 μm wide, perpendicular to the crack. Scattered light normal to the surface from this area was collected and imaged, through an interference filter, onto the entrance slit of a single monochromator, and detected by a 2-D detector. The spatial resolution was found to be ~30 μm in the MS grade material and ~50 μm in the TS grade material.

The Raman spectrum of PSZ is a linear superposition of the spectra of the (metastable) tetragonal and monoclinic phases. The observed spectra were fitted in real time to a linear combination of previously recorded tetragonal and monoclinic calibration spectra [29, 30]. The result is a profile of the extent of transformation

$$F_m = \frac{f_m}{f_m + f_t} \quad (3)$$

where f_m and f_t are the fractions of the monoclinic and tetragonal phases, respectively.

4. Experimental results

Results of the cyclic fatigue tests (Fig. 3) show the MS grade materials to exhibit lower cyclic fatigue thresholds than the TS grade materials; this is to be expected as threshold values in PSZ generally scale with toughness [10]. The effect of grain size, however, is somewhat difficult to ascertain; while the 32 μm grain size material exhibited higher crack-growth rates in both the MS and TS materials, the 50 and 100 μm grain size materials exhibited similar behaviour.

The incidence of crack arrest did show a consistent variation with grain size. In the 32 μm material, crack growth appeared to be continuous (to within the resolution of crack length measurement), whereas in the other grain-sized materials, crack growth tended to occur in a stepwise fashion with the crack tip regularly making jumps and then periodically arresting. This pattern was especially pronounced in the MS grade materials where crack jumps were approximately a grain diameter in length.

Fig. 4 shows the crack-resistance K_R (Δa) curves for all materials. Again, as expected, the TS grade materials showed higher plateau values than the MS grade materials. The 100 TS grade material exhibited plateau toughness well in excess of those previously reported for long cracks in Mg–PSZ materials. An interesting feature of the R-curves for the highest toughness 50 TS and 100 TS materials is that they rise up to a peak value and then fall gradually. This feature is consistent with theoretical predictions for the effects of phase-transformation toughening [32–34], but has not previously been shown experimentally.

Maps of the transformed zone in all samples, both after the initial fatigue crack and R-curve tests (except for the 32 MS fatigue crack), were obtained; representative maps are shown in Fig. 5 for the 100 TS sample. In all cases, the amount of "background" (i.e. far from the crack) monoclinic fraction decreases after annealing, presumably due to thermal retransformation of monoclinic to tetragonal phase. The half-zone width, H, of the transformed zone was determined from the Raman map; results are summarized in Table I.

A number of features can be discerned from the Raman spectroscopy data. Firstly, the width of the transformed zones as a result of cyclic loading was approximately half that exhibited as a result of monotonic loading during the R-curve tests. The size of the transformed zone, as indicated by the zone height, H, has been shown to be directly dependent on the applied stress intensity K, specifically $H \propto K^2$ [23]. The higher values of K applied during R-curve testing clearly result in larger transformation-zone sizes as well as a greater extent of transformations near the crack faces. Under cyclic loading, the lower applied K (K_{max} of the loading cycle) results in less phase transformation and smaller zone widths. An example of this can be seen in Fig. 5a and b which show the percentage of monoclinic phase around the crack as a result of cyclic and monoclinic crack growth in the 100 TS sample.

Secondly, as can be seen in Fig. 5b, the heat treatment was successful in retransforming the monoclinic phase near the crack back to its original tetragonal phase. This enabled crack-resistance curves to be obtained from a sharp through-thickness crack. This procedure permits a better indication of the crack-resistance behaviour in the early stages of crack extension compared to data obtained from a blunt notch or after fatigue precracking where the cyclically induced transformed zone is not removed [10].

Note finally that, in all cases, the cyclic fatigue cracks were grown under decreasing applied stress–intensity conditions. Inspection of the transformed zone widths, however, revealed them to be

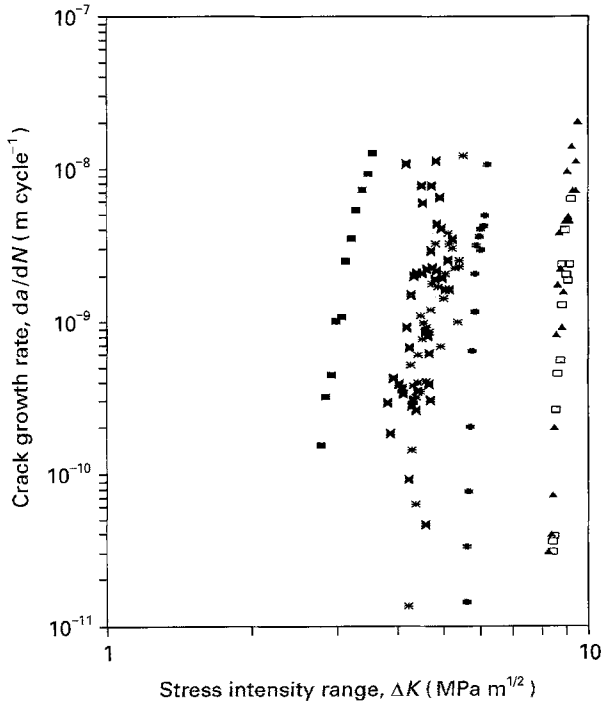

Figure 3 Variation in cyclic fatigue–crack growth rates da/dN as a function of applied stress–intensity range, ΔK, for Mg–PSZ. ■ 32 MS; + 32 TS; * 50 MS; □ 50 TS; × 100 MS; ▲ 100 TS.

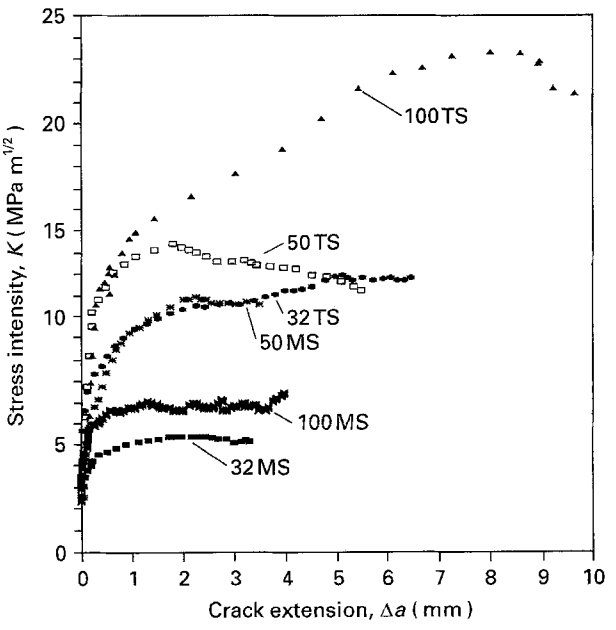

Figure 4 Crack-resistance curves for Mg–PSZ (MS and TS grades) with varying grain size. See Fig. 3 for key.

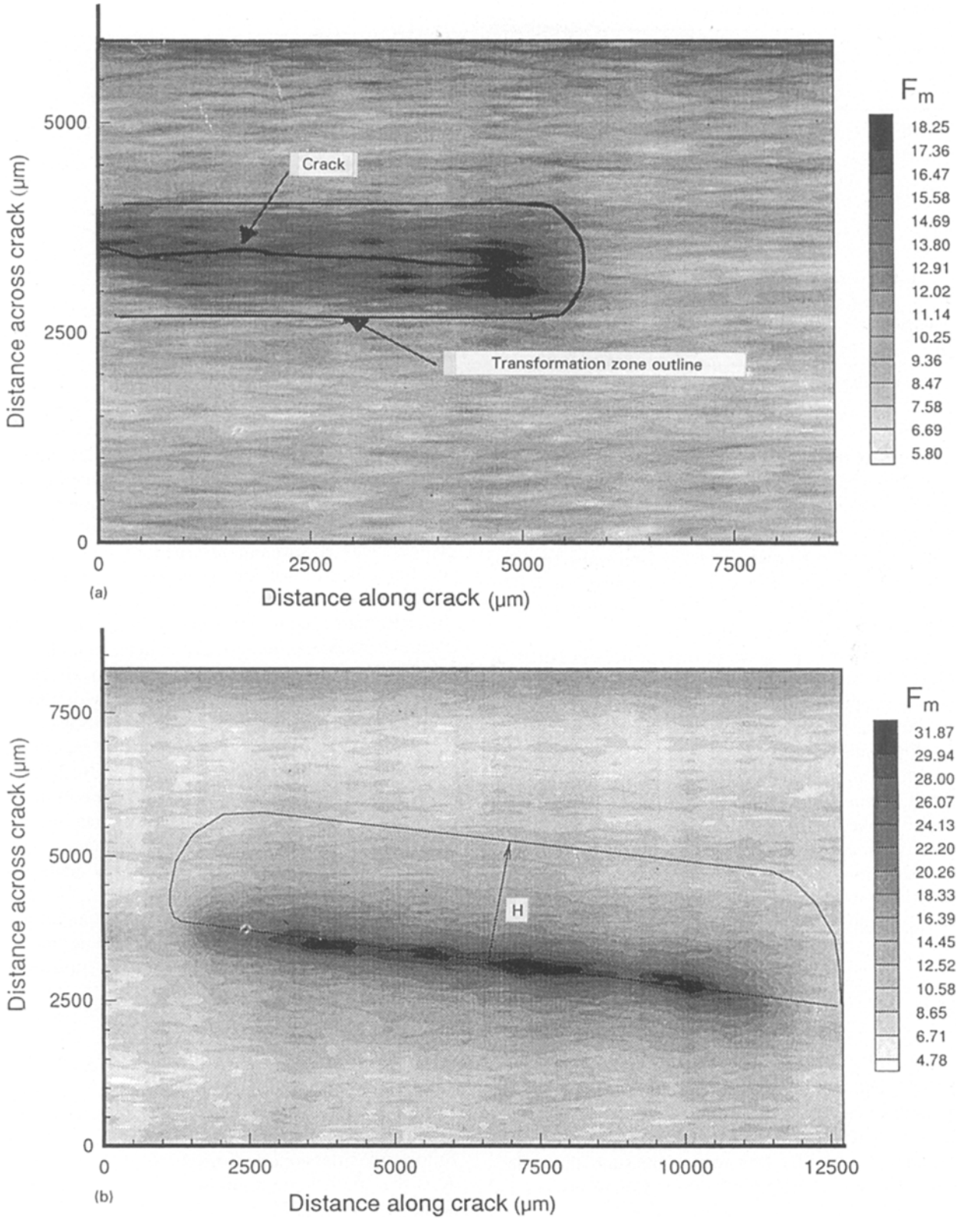

Figure 5 Results of Raman spectroscopy for the 100 TS material showing transformation zones around (a) a cyclically grown crack and (b) a crack grown under monotonic load, showing zone profile used in modelling.

approximately constant in width. This is believed to be due to the steepness of the crack-growth curves, i.e. the very large crack-growth exponents result in only a small variation in K_{max} during the fatigue test.

5. Analysis

It is clear by comparison of results for MS and TS grade materials that, similar to previously reported behaviour [10], increased crack-tip shielding from transformation toughening also increases cyclic fatigue–crack growth thresholds. With respect to the effects of grain size on fatigue–crack growth behaviour, consideration will first be given to the effect of transformation shielding of the crack tip.

The stress intensity at the crack tip, K_{tip}, may be expressed as

$$K_{tip} = K - K_s \quad (4)$$

TABLE I Summary of Raman spectroscopy data

Sample	Description	Half-zone width, H (mm)	Map width (mm)	Map length (mm)	No. of profiles	Raman spectra per profile	β[a]
32 MS	R-curve	0.48	5.08	7.86	40	150	0.46
50 MS	Fatigue-crack	0.43	2.64	0.66	25	130	
	R-curve	0.70	5.08	16.46	99	150	0.74
100 MS	Fatigue crack	0.37	2.64	12.64	49	130	
	R-curve	0.60	5.08	14.79	45	150	0.57
32 TS	Fatigue crack	0.92	6.11	7.79	25	130	
	R-curve	1.07	7.34	12.44	40	130	0.67
50 TS	Fatigue crack	0.86	6.11	6.45	20	130	
	R-curve	2.20	8.13	14.09	60	144	0.71
100 TS	Fatigue crack	0.78	6.11	8.70	25	130	
	R-curve	2.12	8.47	13.30	40	150	0.82

[a] from Equation 11.

where K is the applied stress intensity and K_s represents the extent of crack-tip shielding. In Mg–PSZ, the major contribution to K_s is from transformation toughening, however, crack-tip shielding from other sources, such as crack bridging, may also provide some contribution. For our initial analysis it will be assumed that phase-transformation toughening is the sole source of crack-tip shielding.

Previous work [10] has shown the presence of crack closure during cyclic fatigue; the resulting crack wedging causes premature contact between the crack surfaces and raises the minimum stress intensity of the loading cycle, K_{min}, to K_{cl}, the applied stress intensity at which the crack surfaces come into contact. As stress intensities at the crack tip are different from those applied in the far field, it is necessary to adapt traditional expressions of cyclic fatigue–crack growth as a function of applied stress–intensity range, ΔK, to functions of the stress–intensity range at the crack tip, ΔK_{tip}, where

$$\Delta K_{tip} = (K_{tip})^{max} - (K_{tip})^{min} \quad (5)$$

and

$$(K_{tip})^{min} = K_{cl} - K_s \quad (6)$$

It has been found [10] that while crack closure as a result of crack surface roughness does occur, initial closure near the crack tip is due to dilational strains associated with the transformation such that effectively $K_{cl} \approx K_s$. Therefore by using Equations 5 and 6

$$\Delta K_{tip} = (K_{tip})^{max} \quad (7)$$

$$\Delta K_{tip} = (K)^{max} - K_s \quad (8)$$

The extent of crack-tip shielding due to the dilational component of the phase transformation may be expressed as [33]

$$K_s = \frac{E}{3\sqrt{2}\pi(1-\nu)} \iint_A \theta r(\Phi)^{-3/2} \cos\left(\frac{3}{2}\Phi\right) dA \quad (9)$$

where A is the transformed region, ν is Poisson's ratio (≈ 0.31), E is Young's modulus (≈ 207 GPa) and θ is the product of the volume fraction of the transformed phase, i.e. the tetragonal phase (≈ 0.25), and the dilatant strain (≈ 0.04). θ varies as a function of the angular radius of the zone, $r(\Phi)$, as shown by the Raman spectroscopy data. In this formulation, long range shear strains are assumed to be relieved by twinning. In practice, then if the extent of transformation is known for regions surrounding the crack (e.g. from Raman spectroscopy measurements), Equation 9 can be evaluated numerically to determine the value of K_s. The advantage of this approach is that the extent of transformation toughening is determined directly from the dilational transformation strains. Note, however, that previously reported calculations of K_s using this approach for Mg–PSZ [10, 23], yield values smaller than the measured toughness indicating that either other sources of toughening are operating (e.g. grain or uncracked ligament bridging) or significant shielding is present from shear components of the transformation strain.

Alternatively, for a steady-state zone configuration, i.e. for a crack growing at a constant applied K, evaluation of Equation 9 for a uniformly transformed zone of constant θ and width H yields

$$K_s = \alpha\theta E H^{\frac{1}{2}} \quad (10)$$

where H is the half-height of the zone and α is a constant defined by the frontal zone shape. For a transformation triggered by some critical transformation stress, σ_c, associated with the applied stress field, it follows that the zone half-height $H \propto (K/\sigma_c)^2$ where K is the applied stress intensity, and therefore using Equation 10 [10, 23]

$$K_s = \beta K \quad (11)$$

where β is a material constant. For a non-uniformly transformed zone where the extent of transformation decreases from the crack surfaces to the outer edge of the transformed zone as seen in the Raman spectroscopy measurements, Equations 10 and 11 may still be applied provided that lines of constant transformation strain are geometrically self-similar with the outer boundary of the transformed zone. In addition, Equation 11 may be used to provide an estimate of transformation shielding from zones formed around cracks grown under cyclic loading conditions. Previous work

has shown that the extent of transformation toughening from cyclic and monotonic loading does not differ significantly [10, 23].

For the present materials the values of β are determined from the steady-state (or plateau) K_c and initiation (or intrinsic) K_0 toughness values from the R-curve tests using Equations 4 and 11; values are reported in Table I. Using these values of β together with Equations 8 and 11, crack-growth rates are replotted in Fig. 6 as a function of the crack-tip stress intensity range ΔK_{tip}. Note, however, that with this estimation of K_s it is not possible to separate out contributions to toughening from other sources (such as crack bridging), as noted above.

6. Discussion

Cyclic fatigue–crack growth rates independent of transformation crack-tip shielding (and possibly other sources of toughening) can be seen in Fig. 6 plotted as a function of ΔK_{tip}. The fatigue thresholds for the MS grade materials are on average below those of the TS grade materials but close to values previously reported for a similar MS grade PSZ [10].

Cyclic fatigue is observed to occur at crack-tip stress intensities typically in the range of 60 ~ 70% of the intrinsic toughness K_0. Thus the near-tip thresholds for fatigue–crack growth, $(\Delta K_{tip})_{TH}$, appear to scale with K_0 values of ~3 and ~4 MPa $m^{\frac{1}{2}}$ for the MS and TS grade materials, respectively. Fig. 7 shows the near-tip fatigue data normalized with respect to K_0. While there is a degree of scatter, all the materials tested show similar crack-growth behaviour.

It therefore appears that the mechanism of cyclic fatigue–crack growth is essentially unaffected by changes in grain size. Since crack growth is predominantly transgranular this might not immediately seem surprising. In other monolithic ceramics where crack growth is more intergranular and grain bridging occurs, crack-growth rates are found to be sensitive to grain size [5, 14]. However, for the present Mg–PSZ, other microstructural features are expected to vary with grain size and might also be expected to affect fatigue crack-growth behaviour. These may include variation in the grain boundary phases, localized residual stresses and associated variations in the extent of microcracking ahead of the crack tip and unbroken ligaments left in the wake of the crack. Within the scatter observed in the growth-rate data of Fig. 7, however, no major effects are apparent. (Scatter in the growth-rate data curves on the abscissa could usually be traced to variations in the background monoclinic phase measured using Raman spectroscopy prior to and after the heat treatments used to retransform the monoclinic phase.) This also confirms previous work [35] showing that cyclic fatigue thresholds scale directly with the volume fraction of tetragonal and delta ($Mg_2Zr_5O_{12}$) phases independent of other microstructural variations.

Comparisons of the near-tip crack-growth data with similar data for environmentally-assisted crack growth under sustained loads would provide some indication as to whether intrinsic mechanisms for

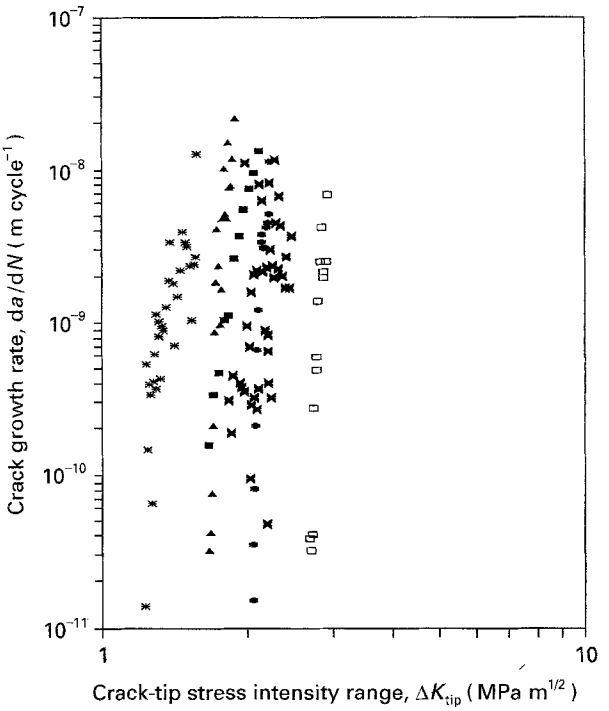

Figure 6 Cyclic fatigue–crack growth rates as a function of the local stress–intensity range at the crack tip, ΔK_{tip}, for Mg–PSZ. See Fig. 3 for key.

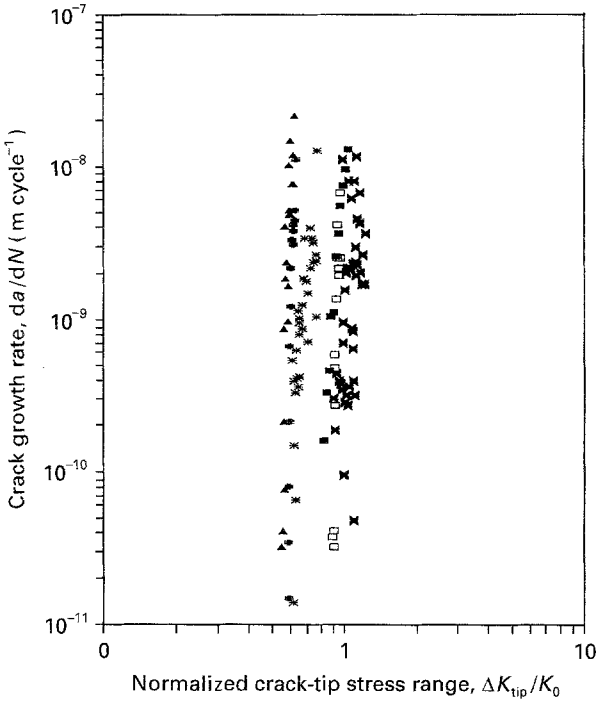

Figure 7 Cyclic fatigue-crack growth rates in Mg–PSZ as a function of stress–intensity range at the crack tip, ΔK_{tip}, normalized with respect to the intrinsic fracture toughness, K_0. See Fig. 3 for key.

fatigue–crack growth were operating under cyclic loads. While such data were not measured in the present study, previously reported environmentally assisted crack-growth data [10, 36] for the same 50 μm grain size MS grade PSZ material do facilitate comparison. Results of the previous and present studies are presented in Fig. 8. It is apparent from the figure that cyclic crack growth may occur at crack-tip

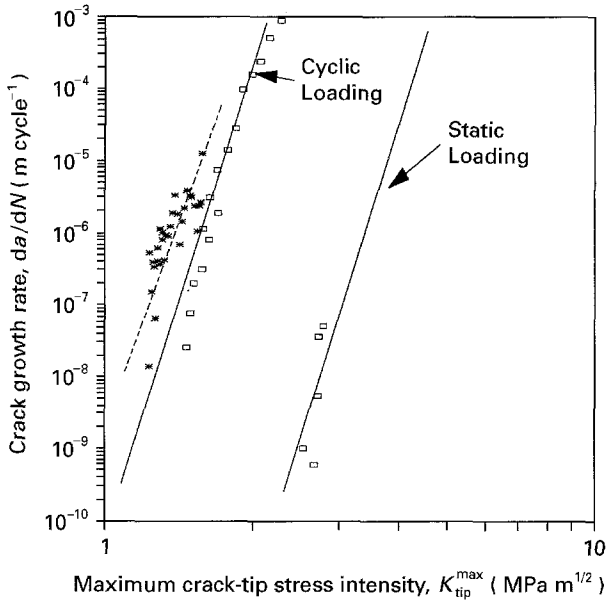

Figure 8 Comparison of crack-growth rates in 50 MS grade Mg–PSZ as a function of the near-tip stress intensity (K_{tip} of the applied K under cyclic loads) under sustained and cyclic loads. Environmentally-assisted crack-growth data taken from a previous study [10, 35] was observed to occur at higher K_{tip} values. □ previous work; * 50 MS.

stress intensities *lower* than those required for crack growth under sustained loads. Based on these observations, it appears that in Mg–PSZ ceramics, an intrinsic mechanism associated with cyclic loading may contribute to fatigue–crack advance at crack-tip stress intensities lower than those required for mechanisms of slow crack growth (stress–corrosion cracking). Alternatively, more recent high-resolution scanning electron microscopy observations by one of the authors [37] indicate that a near-tip bridging zone is formed by both randomly distributed large precipitates and the smaller regular lens-shaped tetragonal precipitates (maximum dimension ~200 nm). Frictional sliding and associated wear degradation of these bridging precipitates under cyclic loading may provide an extrinsic mechanism for fatigue-crack growth similar to previously reported grain-bridging models [5, 14]. Confirmation of a fatigue mechanism, however, awaits confirmation from further crack-growth data, careful analysis of the extent of transformation toughening and improved imaging of the near-tip microstructure.

7. Conclusions

Six different Mg–PSZ materials were tested with three different cubic-phase grain sizes and two different heat treatment conditions. Cyclic fatigue–crack growth and crack-resistance curve measurements were performed, with Raman spectroscopy used to observe *in situ* phase changes. The following conclusions can be made:

1. Cyclic fatigue-crack growth and fatigue thresholds in Mg–PSZ were found to be strongly dependent on the degree of crack-tip shielding due to phase transformation.
2. The mechanisms responsible for cyclic fatigue-crack growth appeared to be independent of grain size.
3. Preliminary comparisons of the crack-growth rate dependence on the crack-tip stress intensity under cyclic and sustained loads appear to indicate that intrinsic fatigue mechanisms may contribute to crack advance under cyclic loads, although the contribution from an extrinsic mechanism involving frictional-wear degradation of near-tip bridging by tetragonal precipitates remains to be examined.

Acknowledgements

Experimental studies at the Lawrence Berkeley Laboratory were supported by the Director, Office of Energy Research, Office of Basic Energy Sciences, Materials Sciences Division of the U.S. Department of Energy under Contract No. DE-AC03-76SF00098. The authors would like to thank ICI Advanced Ceramics for supply of the material and support of the work. Thanks also to the Australian Research Council. MJH is currently supported by an APRA (Industry).

References

1. A. G. EVANS and E. R. FULLER, *Metall. Trans.* **50** (1974) 27.
2. A. G. EVANS, *Int. J. Fracture* **16** (1980) 485.
3. M. J. REECE, F. GUIU and M. F. R. SAMMUR, *J. Amer. Ceram. Soc.* **72** (1989) 348.
4. L. EWART and S. SURESH *J. Mater. Sci.* **22** (1987) 1173.
5. S. LATHABAI, J. RÖDEL and B. R. LAWN, *J. Amer. Ceram. Soc.* **74** (1991) 1340.
6. M. MASUDA, T. SOMA, M. MATSUI and I. ODA, *J. Eur. Ceram. Soc.* **6** (1990) 253.
7. M. V. SWAIN and V. ZELIZKO, *Adv. Ceram.* **24** (1988) 595.
8. M. J. HOFFMAN, W. LENTZ, M. V. SWAIN and Y.-W. MAI, *J. Eur. Ceram. Soc.* **11** (1992) 445.
9. R. H. DAUSKARDT, W. YU and R.O. RITCHIE, *J. Amer. Ceram. Soc.* **70** (1987) C248.
10. R. H. DAUSKARDT, D. B. MARSHALL and R.O. RITCHIE, *Ibid.* **73** (1990) 893.
11. S. LATHABAI, Y.-W. MAI and B. R. LAWN, *Ibid.* **72** (1989) 1760.
12. X. -Z. HU and Y.-W. MAI, *Ibid.* **75** (1992) 848.
13. X. -Z. HU, Y.-W. MAI and S. LATHABAI, *J. Eur. Ceram. Soc.* **9** (1992) 213.
14. R. H. DAUSKARDT, *Acta Metall Mater* **41** (1993) 2765.
15. D. DAVIDSON, J. B. CAMPBELL and J. LANKFORD, *Ibid.* **39** (1991) 1319.
16. S. -Y. LIU and I-W. CHEN, *J. Amer. Ceram. Soc.* **74** (1991) 1206.
17. M. J. HOFFMAN, R. H. DAUSKARDT, Y. -W. MAI and R.O. RITCHIE, "in Science and Technology of Zirconia V," edited by S.P.S. Badwal, M.J. Bannister, and R.H.J. Hannink (Technomic Publishing Co., Lancaster, PA, 1993) 321.
18. T. LIN, A. G. EVANS and R. O. RITCHIE, *Acta Metall.* **34** (1986) 2205.
19. J. -K. SHANG and R. O. RITCHIE, *Metall. Trans A*, **20A** (1989) 897.
20. S. -Y. LIU and I-W. CHEN, *J. Amer. Ceram. Soc.* **74** (1991) 1197.
21. A. H. HEUER, M. RÜHLE and D. B. MARSHALL, *Ibid.* **73** (1990) 1084.
22. D. B. MARSHALL and M. V. SWAIN, *J. Amer. Ceram. Soc.* **71** (1988) 399.
23. D. B. MARSHALL, M. C. SHAW, R. H. DAUSKARDT, R. O. RITCHIE, M. J. READEY and A. H. HEUER, *Ibid.* **73** (1990) 2659.

24. F. GUIU, M. J. REECE and D. A. J. VAUGHAN, in "Fatigue of Advanced Materials", edited by R.O. Ritchie, R.H. Dauskardt and B.N. Cox (MCEP Publishing Ltd., Edgbaston, UK 1991) p. 193.
25. H. N. KO, *J. Mater. Sci. Lett.* **8** (1989) 1438.
26. T. LIU, R. MATT and G. GRATHWOHL, *J. Mater. Design.* **14** (1993) 159.
27. T. LIU and Y. -W. MAI, *J. Amer. Ceram. Soc.* **76** (1993) 2601.
28. G. H. SIH, "Handbook of stress intensity factors," 1.5.1–1 (1973).
29. R. H. DAUSKARDT, D. K. VEIRS and R. O. RITCHIE, *J. Amer. Ceram. Soc.* **72** (1989) 1124.
30. D. K. VEIRS, J. W. AGER, III, E. T. LOUCKS and G. M. ROSENBLATT, *Appl. Optics* **29** (1990) 4969.
31. D. K. VEIRS, J. W. AGER, III and G. M. ROSENBLATT, *Ceram. Trans.* **19** (1991) 1043.
32. D. M. STUMP and B. BUDIANSKY, *Acta Metall.* **37** (1989) 3297.
33. B. BUDIANSKY, J. W. HUTCHINSON and J. C. LAMBROPOULOS, *Int. J. Solids Struct.* **19** (1983) 337.
34. D. M. STUMP and B. BUDIANSKY, *Ibid.* **25** (1989) 635.
35. M. HOFFMAN and Y. -W. MAI, in "Structural Ceramics", Proceedings of IUMRS, International Meeting of Advanced Materials, Japan (Materials Research Society, Pittsburg, PA, 1993) p. 365.
36. R. H. DAUSKARDT, W. C. CARTER, D. K. VEIRS and R. O. RITCHIE, *Acta Metall. Mater.* **38** (1990) 2327.
37. M. J. HOFFMAN and S. WAKAYAMA, Tokyo Metropolitan University, Tokyo, Japan (1993), unpublished data.

Received 23 November
and accepted 25 November 1994